Nonautonomous matter waves in a spin-1 Bose-Einstein condensate

Yu-Jia Shen,[1] Yi-Tian Gao,[1,*] Da-Wei Zuo,[1,2] Yu-Hao Sun,[1] Yu-Jie Feng,[1] and Long Xue[1]
[1]*Ministry-of-Education Key Laboratory of Fluid Mechanics and National Laboratory for Computational Fluid Dynamics, Beijing University of Aeronautics and Astronautics, Beijing 100191, China*
[2]*Department of Mathematics and Physics, Shijiazhuang Tiedao University, Shijiazhuang 050043, China*
(Received 25 March 2014; published 13 June 2014)

To investigate nonautonomous matter waves with time-dependent modulation in a one-dimensional trapped spin-1 Bose-Einstein condensate, we hereby work on the generalized three-coupled Gross-Pitaevskii equations by means of the Hirota bilinear method. By modulating the external trap potential, atom gain or loss, and coupling coefficients, we can obtain several nonautonomous matter-wave solitons and rogue waves including "bright" and "dark" shapes and arrive at the following conclusions: (i) the external trap potential and atom gain or loss can influence the propagation of matter-wave solitons and the duration and frequency of bound solitonic interaction, but they have little effect on the head-on solitonic interaction; (ii) through numerical simulation, stable evolution of the matter-wave solitons is realized with a perturbation of 5% initial random noise, and the spin-exchange interaction of atoms can be affected by the time-dependent modulation; (iii) under the influence of a periodically modulated trap potential and periodic atom gain or loss, rogue waves can emerge in the superposition of localized character and periodic oscillating properties.

DOI: 10.1103/PhysRevE.89.062915   PACS number(s): 05.45.Yv, 03.75.Lm, 31.15.−p

I. INTRODUCTION

As a phenomenon existing in condensed matter, atomic, nuclear, and particle physics [1], the Bose-Einstein condensate (BEC) has been observed in a vapor of rubidium-87 atoms confined by a magnetic field [2] and also has been produced in certain atomic gases such as of sodium, lithium, hydrogen, helium, and potassium atoms [3–7]. In magnetic traps, the atoms that carry spins still behave like scalar particles, because the spin degree of freedom is constrained [1–8].

Since a sodium atom BEC has been confined in an optical dipole trap, restrictions of magnetic traps can be eliminated [8]. In contrast with magnetic traps, the spin of atoms is proven to be free in optical traps [8–11]. Therefore, we can investigate the spinor properties of such a BEC, including its ground-state structures with interaction parameters and the spin waves and vortices in the condensed atomic gas [9–11]. For instance, in the spin-1 atomic BEC, the energetic and dynamic stabilities of coreless vortices trapped with a three-dimensional optical potential and a Ioffe-Pritchard field have been studied [12]. Homogeneous stationary states with their existence, bifurcations, and energy spectra in the spin-1 BEC have been analyzed [13]. In addition, production of matter-wave solitons in the BEC of lithium atoms have been reported, while propagation and interaction of the solitons have been observed [14,15].

The spin-1 BEC can be described via a macroscopic wave function $\Psi = (\Psi_1, \Psi_0, \Psi_{-1})^T$ with three components, Ψ_j $(j = -1, 0, 1)$, and the mean-field Hamiltonian can be written as [9–11,16,17]

$$H = \int d\mathbf{r} \left\{ \sum_{j=-1}^{1} \Psi_j^* \left[-\frac{\hbar^2}{2M}\nabla^2 + U_{\text{trap}}(\mathbf{r}) \right] \Psi_j + \frac{\overline{c}_0}{2} n_0^2 + \frac{\overline{c}_2}{2} |\mathbf{F}|^2 \right\}, \tag{1}$$

where the superscript T denotes the transpose, $*$ denotes the complex conjugate, ∇^2 is the Laplacian, $\hbar$ is the reduced Planck constant, $\mathbf{r}$ is the relative space coordinate vector including three components $\widehat{x}$, $\widehat{y}$, and $\widehat{z}$, M is the atomic mass, $U_{\text{trap}}(\mathbf{r})$ stands for the external trap potential, the particle density is $n_0 = |\Psi_1|^2 + |\Psi_0|^2 + |\Psi_{-1}|^2$, the spin density vector is $\mathbf{F} = (F^{\widehat{x}}, F^{\widehat{y}}, F^{\widehat{z}})$ defined by $F^{\vartheta} = \sum_{j_1,\, j_2=-1}^{1} \Psi_{j_1}^* f_{j_1 j_2}^{\vartheta} \Psi_{j_2}$ with $f_{j_1 j_2}^{\vartheta}$ represented as the element at the j_1-th row and j_2-th column of the spin-1 rotational matrix f^{ϑ} ($\vartheta = \widehat{x}, \widehat{y}$, or $\widehat{z}$), and the coupling constants $\overline{c}_0 = (\overline{g}_0 + 2\,\overline{g}_2)/3$ and $\overline{c}_2 = (\overline{g}_2 - \overline{g}_0)/3$ denote the mean-field and spin-exchange interaction, with $\overline{g}_{\mathscr{F}}$ related to the corresponding s-wave scattering length $a_{\mathscr{F}}$ of the total hyperfine spin $\mathscr{F} = 0, 2$ channels as $\overline{g}_{\mathscr{F}} = 4\pi\hbar^2 a_{\mathscr{F}}/M$ [11,17,18]. Deduced from a variational principle $i\,\hbar\,\partial_{t'}\Psi_j = \delta H/\delta\Psi_j^*$ [11,17,18], the evolution of spinor wave functions in the quasi-one-dimensional spin-1 BEC with the external potential $U_{\text{trap}}(\mathbf{r}) = 0$ can be expressed as the following coupled nonlinear Gross-Pitaevskii (GP) equations [11,17,18]:

$$i\,\hbar\,\partial_{t'}\Psi_1 = -\frac{\hbar^2}{2M}\,\partial_{x'}^2\Psi_1 + (c_0 + c_2)\,(|\Psi_1|^2 + |\Psi_0|^2)\,\Psi_1 + (c_0 - c_2)\,|\Psi_{-1}|^2\Psi_1 + c_2\Psi_0^2\,\Psi_{-1}^*, \tag{2a}$$

$$i\,\hbar\,\partial_{t'}\Psi_0 = -\frac{\hbar^2}{2M}\,\partial_{x'}^2\Psi_0 + (c_0 + c_2)\,(|\Psi_1|^2 + |\Psi_{-1}|^2)\,\Psi_0 + c_0\,|\Psi_0|^2\Psi_0 + 2\,c_2\Psi_1\Psi_{-1}\Psi_0^*, \tag{2b}$$

$$i\,\hbar\,\partial_{t'}\Psi_{-1} = -\frac{\hbar^2}{2M}\,\partial_{x'}^2\Psi_{-1} + (c_0 + c_2)\,(|\Psi_0|^2 + |\Psi_{-1}|^2)\,\Psi_{-1} + (c_0 - c_2)\,|\Psi_1|^2\Psi_{-1} + c_2\Psi_0^2\,\Psi_1^*, \tag{2c}$$

where δ denotes the functional derivative, i is the imaginary unit, x' and t' are the scaled space and time coordinates, while the one-dimensional coupling constants are $c_0 = (g_0 + 2g_2)/3$ and $c_2 = (g_2 - g_0)/3$, with the modified $g_{\mathscr{F}}$ represented as [11,17,18]

$$g_{\mathscr{F}} = \frac{4\,\hbar^2 a_{\mathscr{F}}}{M a_\perp^2}\,\frac{1}{1 - C(a_{\mathscr{F}}/a_\perp)}, \quad \mathscr{F} = 0, 2, \tag{3}$$

*Corresponding author: gaoyt@public.bta.net.cn

$C = -\zeta(1/2) \approx 1.46$, ζ as the Riemann zeta function, and $a_\perp$ as the size of the ground state in relative transverse motion [11,17,18]. For the dynamic properties of Eqs. (2), an integrable case has been proposed with the coupling constants $c_0 = c_2 \equiv -\kappa < 0$ [18–20]. Through the transformations $\mathbf{\Psi} = (\Psi_1, \Psi_0, \Psi_{-1})^T \to (\psi_1, \sqrt{2}\,\psi_0, \psi_{-1})^T$, $t = \kappa\, t'/\hbar$, and $x = x'\sqrt{2M\kappa}/\hbar$, Eqs. (2) can be rewritten in dimensionless forms as [18–21]

$$i\,\psi_{1,t} + \psi_{1,xx} + 2\,(|\psi_1|^2 + 2\,|\psi_0|^2)\,\psi_1 + 2\,\psi_0^2\,\psi_{-1}^* = 0, \tag{4a}$$

$$i\,\psi_{0,t} + \psi_{0,xx} + 2\,(|\psi_1|^2 + |\psi_0|^2 + |\psi_{-1}|^2)\,\psi_0 + 2\,\psi_1\psi_{-1}\psi_0^* = 0, \tag{4b}$$

$$i\,\psi_{-1,t} + \psi_{-1,xx} + 2\,(|\psi_{-1}|^2 + 2\,|\psi_0|^2)\,\psi_{-1} + 2\,\psi_0^2\,\psi_1^* = 0, \tag{4c}$$

where ψ_j $(j = -1, 0, 1)$ are the three components of the relative wave function $\mathbf{\Psi}$ with the scaled space coordinate x and time t. By means of the Hirota bilinear method and Darboux transformation, multisoliton and rogue-wave solutions of Eqs. (4) have been derived [18,20,21], and the interaction between the polar and ferromagnetic solitons without the effect of the external trap potential has also been illustrated [18,20].

From the experiments of two-body interactions in BECs, a tunable resonance structure, called the Feshbach resonance, has been observed in the cross sections for elastic and inelastic interactions of ultracold atoms [22–30]. The Feshbach resonance occurs when the energy of a molecular (quasi-)bound state is tuned to the energy of two interacting atoms with an external field, which leads to the observed modification of the atomic scattering length and provides remarkable opportunities for the study of nonautonomous matter waves in the BEC with tuned interatomic interaction [22–30]. Nonautonomous matter waves subjected to a certain external time-dependent force have several features that differ from those of classical matter waves in an autonomous system, which extend the concept of matter waves and have been investigated in nonspin BEC [31–41]. In this paper, we will focus our attention on the properties of nonautonomous matter waves in trapped spin-1 BECs by tuning the interatomic interaction near the Feshbach resonance. Thus, we consider the generalized nonautonomous system

$$\begin{aligned} i\,\psi_{1,t} = {} & -\psi_{1,xx} + [U_{\text{trap}}(x,t) + i\,\Gamma(t)]\psi_1 \\ & + \big[A_1^{(1)}(t)\,|\psi_1|^2 + A_0^{(1)}(t)\,|\psi_0|^2 + A_{-1}^{(1)}(t)\,|\psi_{-1}|^2\big]\psi_1 \\ & + C_1(t)\,\psi_0^2\,\psi_{-1}^*, \end{aligned} \tag{5a}$$

$$\begin{aligned} i\,\psi_{0,t} = {} & -\psi_{0,xx} + [U_{\text{trap}}(x,t) + i\,\Gamma(t)]\psi_0 \\ & + \big[A_1^{(0)}(t)\,|\psi_1|^2 + A_0^{(0)}(t)\,|\psi_0|^2 + A_{-1}^{(0)}(t)\,|\psi_{-1}|^2\big]\psi_0 \\ & + C_0(t)\,\psi_1\,\psi_{-1}\,\psi_0^*, \end{aligned} \tag{5b}$$

$$\begin{aligned} i\,\psi_{-1,t} = {} & -\psi_{-1,xx} + [U_{\text{trap}}(x,t) + i\,\Gamma(t)]\psi_{-1} \\ & + \big[A_1^{(-1)}(t)\,|\psi_1|^2 + A_0^{(-1)}(t)\,|\psi_0|^2 \\ & + A_{-1}^{(-1)}(t)\,|\psi_{-1}|^2\big]\psi_{-1} + C_{-1}(t)\,\psi_0^2\,\psi_1^*, \end{aligned} \tag{5c}$$

which is the mean-field approximation for the dynamics of the one-dimensional trapped spin-1 BEC. Here $U_{\text{trap}}(x,t)$ represents the time-dependent external trap potential [31–37], the time-dependent gain or loss term $\Gamma(t)$ corresponds to the mechanism of loading external atoms into the BEC through optical pumping or depleting atoms from the BEC continuously [31–34,42], and the coupling coefficients $A_{j_2}^{(j_1)}(t)$ and $C_{j_1}(t)$ $(j_1, j_2 = -1, 0, 1)$ are related to the atomic scattering length, which can vary if one tunes the interatomic interaction near the Feshbach resonance [31–37]. There are three special cases of Eqs. (5) that should be mentioned:

(i) When $U(t) = \Gamma(t) = A_{-1}^{(1)}(t) = A_1^{(-1)}(t) = 0$, $A_1^{(1)}(t) = A_1^{(0)}(t) = A_0^{(0)}(t) = A_{-1}^{(0)}(t) = A_{-1}^{(-1)}(t) = -2$, $A_0^{(1)}(t) = A_0^{(-1)}(t) = -4$, and $C_1(t) = C_0(t) = C_{-1}(t) = -2$, Eqs. (5) can be reduced to the autonomous system, i.e., Eqs. (4) [18–21].

(ii) When $\psi_0 = 0$, Eqs. (5) can be reduced to two-coupled GP equations in the two-component trapped BEC including the time-dependent gain or loss [31–33]. The bright-soliton and dark-soliton solutions of the two coupled GP equations have been calculated under the influence of several time-dependent external potentials [31–33].

(iii) When $\psi_0 = 0$ and $\psi_1 = \psi_{-1}$, Eqs. (5) can be reduced to the single GP equation that represents the dynamics of one mean-field wave function in the nonspin BEC [34–41]. The Darboux transformation and rogue-wave solutions of the single GP equation have been derived [38–41]. By modulating the time-dependent harmonic oscillator potential, the nonautonomous matter-wave solitons, which interact elastically and propagate with varying amplitudes, speeds, and spectra, have been described [35], and the parametric resonance for solitons has been investigated through numerical simulation [36]. By means of analytical and numerical methods, the features of nonautonomous matter-wave solitons near the Feshbach resonance have been revealed under the effect of time-dependent nonlinearity and external trap potential [37].

However, to our knowledge, the nonautonomous matter waves of Eqs. (5) with the time-dependent external trap potential $U_{\text{trap}}(x,t)$ and gain or loss term $\Gamma(t)$ in the spin-1 BEC have not been widespread as yet. In Sec. II, under some constraints of the variable coefficients that will be derived, Eqs. (5) will be bilinearized through an introduced auxiliary function. Based on the bilinear forms, one- and two-soliton solutions will be derived. Through the different parameters chosen in Sec. III, propagation and interaction of the nonautonomous matter-wave solitons from Eqs. (5) will be illustrated and analyzed under the respective effects of such external trap potentials as the expulsive potential, periodically modulated trap potential, and kink-like-modulated trap potential. In Sec. IV, we will perform numerical simulation to show that the evolution of nonautonomous matter-wave solitons can be stable with a perturbation of 5% random noise via some chosen initial conditions. The spin-exchange interaction of atoms, which is related to the interaction of matter-wave solitons, will also be investigated. In addition, under the same constraints derived in Sec. II, rogue-wave-like solutions of Eqs. (5)

will be obtained in Sec. V; these describe the dynamics of nonautonomous rogue waves, i.e., the rogue waves formed by the accumulation of energy and atoms toward their central part and simultaneously affected by time-dependent nonlinearity and external trap potential [40,41]. Finally, Sec. VI will present our conclusions.

II. BILINEAR FORMS AND SOLITON SOLUTIONS OF EQS. (5)

Particularly, we will, in line with Refs. [31–41], choose the harmonic-like trap potential as

$$U_{\rm trap}(x,t)=U(t)\,x^2 \tag{6}$$

to investigate the effect of external trap potential on the propagation and interaction of the matter-wave solitons. To get the bilinear forms of Eqs. (5), we will present the following constraints on the variable coefficients:

$$A_1^{(1)}(t)=A_1^{(0)}(t)=A_1^{(-1)}(t)+C_{-1}(t)=A_1(t), \tag{7a}$$

$$A_0^{(1)}(t)=A_0^{(0)}(t)+C_0(t)=A_0^{(-1)}(t)=A_0(t), \tag{7b}$$

$$A_{-1}^{(1)}(t)+C_1(t)=A_{-1}^{(0)}(t)=A_{-1}^{(-1)}(t)=A_{-1}(t), \tag{7c}$$

$$U(t)=-\Gamma(t)^2-\frac{1}{2}\,\frac{d\,\Gamma(t)}{dt}. \tag{7d}$$

Through the dependent-variable transformations

$$\psi_j=\frac{G_j}{F}\,e^{\frac{1}{2}\Gamma(t)x^2 i},\quad j=-1,0,1, \tag{8}$$

with the real function F and complex functions G_j $(j=-1,0,1)$ of x and t, we can derive the bilinear forms of Eqs. (5):

$$\begin{aligned} &i\,D_t\,G_j\cdot F+2\,i\,x\,\Gamma(t)D_x\,G_j\cdot F+D_x^2\,G_j\cdot F\\ &\quad=(-1)^{j+1}\,C_j(t)\,S\,G_{-j}^*,\quad j=-1,0,1, \end{aligned} \tag{9a}$$

$$D_x^2\,F\cdot F=-\sum_{j=-1}^{1}A_j(t)\,|G_j|^2, \tag{9b}$$

$$G_0^2-G_1G_{-1}=SF, \tag{9c}$$

by means of an introduced auxiliary function S, and D is the bilinear operator defined as [43]

$$D_x^m\,a(x)\cdot b(x)=\frac{\partial^m}{\partial\widetilde{x}^m}\,a(x+\widetilde{x})\,b(x-\widetilde{x})\bigg|_{\widetilde{x}=0}, \tag{10a}$$

$$D_t^n\,a(t)\cdot b(t)=\frac{\partial^n}{\partial\widetilde{t}^n}\,a(t+\widetilde{t})\,b(t-\widetilde{t})\bigg|_{\widetilde{t}=0}, \tag{10b}$$

where m and n are positive integers, a and b are functions of x and t, while $\widetilde{x}$ and $\widetilde{t}$ stand for the small increments. To obtain some analytic solutions of Eqs. (5), we present the other constraints:

$$A_1(t)=C_{-1}(t)=\alpha_1\,e^{-4\int\Gamma(t)dt}, \tag{11a}$$

$$A_0(t)=2\,C_0(t)=\alpha_0\,e^{-4\int\Gamma(t)dt}, \tag{11b}$$

$$A_{-1}(t)=C_1(t)=\alpha_{-1}\,e^{-4\int\Gamma(t)dt}, \tag{11c}$$

where the α_j $(j=-1,0,1)$ are real parameters. Constraints (7) and (11) indicate the important interconnections of time-dependent nonlinearity and external trap potential and form a sufficient condition which theoretically ensures the existence of nonautonomous matter-wave solintons and rogue waves in the trapped spin-1 BEC. Based on constraints (7) and (11), we can derive one-soliton, two-soliton, and rogue-wave-like solutions below.

First, we expand G_j, F, and S in power series of a small parameter ε as [43]

$$G_j=g_1^{(j)}\varepsilon+g_3^{(j)}\varepsilon^3+g_5^{(j)}\varepsilon^5+\cdots,\qquad j=-1,0,1, \tag{12a}$$

$$F=1+f_2\,\varepsilon^2+f_4\,\varepsilon^4+f_6\,\varepsilon^6+\cdots, \tag{12b}$$

$$S=s_2\,\varepsilon^2+s_4\,\varepsilon^4+s_6\,\varepsilon^6+\cdots, \tag{12c}$$

where $g_m^{(j)}$ $(j=-1,0,1,m=1,3,5,\ldots)$, f_n, and s_n $(n=2,4,6,\ldots)$ are functions of x and t to be determined. Substituting expressions (12) into bilinear forms (9) and collecting the coefficients of ε with the same power, we derive the following cases:

Case 1:

$$G_j=\beta_1^{(j)}e^{\eta_1}+c_{11}^{(j)}e^{2\eta_1+\eta_1^*},\quad j=-1,0,1, \tag{13a}$$

$$F=1+b_{11}\,e^{\eta_1+\eta_1^*}+d_{11}\,e^{2\eta_1+2\eta_1^*}, \tag{13b}$$

$$S=\Omega_1\,e^{2\eta_1}; \tag{13c}$$

Case 2:

$$\begin{aligned} G_j=&\sum_{m=1}^{2}\beta_m^{(j)}e^{\eta_m}+\sum_{m=1}^{2}\sum_{n=1}^{2}c_{mn}^{(j)}e^{2\eta_m+\eta_n^*}\\ &+\sum_{m=1}^{2}\left[\beta_2^{(j)}b_{1m}+\beta_1^{(j)}b_{2m}+c_m^{(j)}\right]e^{\eta_m+\eta_m^*+\eta_{3-m}}\\ &+\sum_{m=1}^{2}\sum_{n=1}^{2}l_{mn}^{(j)}e^{2\eta_m+2\eta_n^*+\eta_{3-m}}\\ &+\sum_{m=1}^{2}l_m^{(j)}e^{\eta_m+\eta_m^*+2\eta_{3-m}+\eta_{3-m}^*}\\ &+\sum_{m=1}^{2}p_m^{(j)}e^{2\eta_m+2\eta_m^*+2\eta_{3-m}+\eta_{3-m}^*},\\ &j=-1,0,1, \end{aligned} \tag{14a}$$

$$\begin{aligned} F=&1+\sum_{m=1}^{2}\sum_{n=1}^{2}b_{mn}\,e^{\eta_m+\eta_n^*}+\sum_{m=1}^{2}\sum_{n=1}^{2}d_{mn}\,e^{2\eta_m+2\eta_n^*}\\ &+\sum_{m=1}^{2}\left(d_m\,e^{2\eta_m+\eta_m^*+\eta_{3-m}^*}+d_m^*\,e^{2\eta_m^*+\eta_m+\eta_{3-m}}\right)\\ &+\sum_{m=1}^{2}\sum_{n=1}^{2}q_{mn}\,e^{2\eta_m+2\eta_n^*+\eta_{3-m}+\eta_{3-n}^*}\\ &+(b_{11}\,b_{22}+b_{12}\,b_{21}+d_0)\,e^{\eta_1+\eta_1^*+\eta_2+\eta_2^*}\\ &+q_0\,e^{2\eta_1+2\eta_1^*+2\eta_2+2\eta_2^*}, \end{aligned} \tag{14b}$$

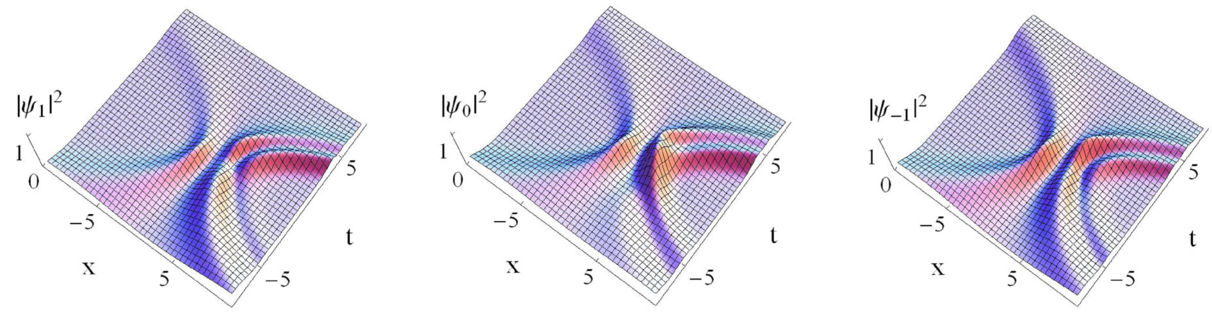

(a) (b) (c)

FIG. 1. (Color online) Head-on interaction between the two solitons formed by $|\psi_j|^2$ ($j = 1,0,-1$) via expressions (8) and (14) with the parameters $\Gamma(t) = \rho_1 \tanh(2\rho_1 t)$, $\tau_1 = 0.8 + 0.4i$, $\tau_2 = 0.5 - 0.6i$, $\beta_1^{(1)} = 0.4$, $\beta_1^{(0)} = 0.5$, $\beta_1^{(-1)} = 0.5$, $\beta_2^{(1)} = 0.4$, $\beta_2^{(0)} = 0.5$, $\beta_2^{(-1)} = 0.625$, $\alpha_1 = \alpha_{-1} = -1$, $w_1^{(0)} = w_2^{(0)} = 0$, and $\rho_1 = 0.15$.

$$S = \Omega_1 e^{2\eta_1} + \Omega_2 e^{2\eta_2} + [\Lambda^{(0,0)} - \Lambda^{(1,-1)}] e^{\eta_1+\eta_2} + \sum_{m=1}^{2}\sum_{n=1}^{2} h_{mn} e^{\eta_m+\eta_n^*+2\eta_{3-m}} + \sum_{m=1}^{2} h_m e^{2\eta_m+2\eta_m^*+2\eta_{3-m}} + h_0 e^{2\eta_1+\eta_1^*+2\eta_2+\eta_2^*}, \tag{14c}$$

where

$$\alpha_0^2 - 4\alpha_1\alpha_{-1} = 0, \tag{15}$$

$$\begin{aligned} \Omega_m &= \left(\beta_m^{(0)}\right)^2 - \beta_m^{(1)}\beta_m^{(-1)}, \\ \eta_m &= k_m(t)\, x + i\, w_m(t), \\ k_m(t) &= \tau_m e^{-2\int \Gamma(t)dt}, \\ w_m(t) &= \int \tau_m^2 e^{-4\int\Gamma(t)dt} dt + w_m^{(0)}, \quad m = 1,2, \end{aligned} \tag{16}$$

$\beta_m^{(j)}$, $w_m^{(0)}$, and τ_m ($j = -1, 0, 1$, $m = 1, 2$) are complex parameters, and the expressions of other quantities above are given in the Appendix due to their lengths. Through transformations (8), expressions (13) and (14) correspond to the one- and two-soliton solutions of Eqs. (5).

III. PROPAGATION AND INTERACTION OF THE MATTER-WAVE SOLITONS UNDER EXTERNAL TRAP POTENTIALS

From the soliton solutions in Sec. II, we can derive the velocities $\widetilde{V}_m$ ($m = 1, 2$) and characteristic lines for the matter-wave solitons as [44,45]

$$\begin{aligned} &\widetilde{V}_m = 2\, x\, \Gamma(t) + (\tau_m - \tau_m^*) e^{-2\int\Gamma(t)dt}, \\ &x\, e^{-2\int\Gamma(t)dt} - (\tau_m - \tau_m^*) \int e^{-4\int\Gamma(t)dt} dt + \frac{\widetilde{c}_m}{\tau_m + \tau_m^*} = 0, \\ &m = 1, 2, \end{aligned} \tag{17}$$

where $\widetilde{c}_m$ ($m = 1, 2$) are the real parameters related to the amplitudes of the relevant matter-wave solitons. Then we will analyze the propagation and interaction of the matter-wave solitons under the respective effects of an expulsive potential, a periodically modulated trap potential, and a kink-like-modulated trap potential as follows.

A. Expulsive potential

For the expulsive parabolic trap potential, i.e., $U(t) = -\rho_1^2$ with ρ_1 a real constant, we can deduce a certain condition $\Gamma(t) = \rho_1 \tanh(2\rho_1 t)$ that the time-dependent gain or loss term meets, and under which the characteristic lines can be written as

$$x\,\mathrm{sech}(2\rho_1 t) - \frac{\tau_m - \tau_m^*}{2\rho_1}\tanh(2\rho_1 t) + \frac{\widetilde{c}_m}{\tau_m + \tau_m^*} = 0, \quad m = 1, 2. \tag{18}$$

From expressions (18), it is seen that the propagation directions of the matter-wave solitons can be affected by the parameter ρ_1 related to the expulsive potential. As shown in Figs. 1 and 2, one soliton in the polar state ($\Omega_1 \neq 0$) and the other in the

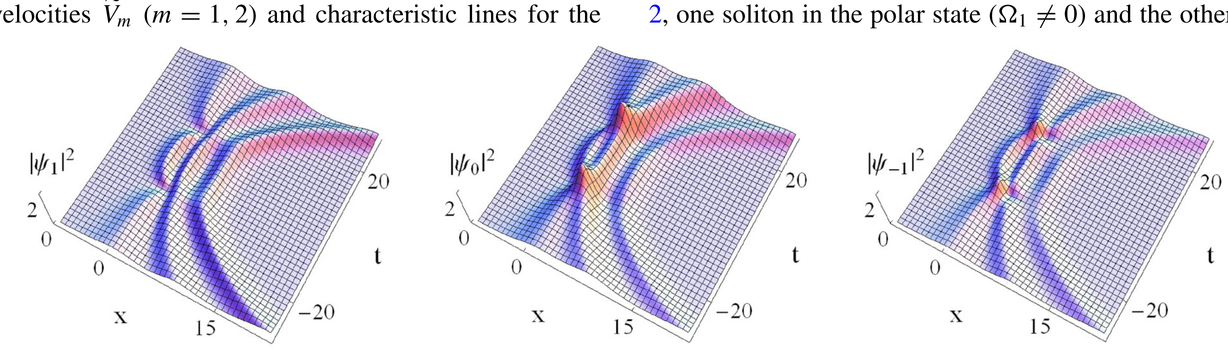

(a) (b) (c)

FIG. 2. (Color online) Bound interaction between the two solitons formed by $|\psi_j|^2$ ($j = 1,0,-1$) via expressions (8) and (14) with the parameters $\Gamma(t) = \rho_1 \tanh(2\rho_1 t)$, $\tau_1 = 1$, $\tau_2 = 0.8$, $\beta_1^{(1)} = 0.4$, $\beta_1^{(0)} = 0.6$, $\beta_1^{(-1)} = 0.5$, $\beta_2^{(1)} = 0.5$, $\beta_2^{(0)} = 0.4$, $\beta_2^{(-1)} = 0.32$, $\alpha_1 = \alpha_{-1} = -1$, $w_1^{(0)} = w_2^{(0)} = 0$, and $\rho_1 = 0.03$.

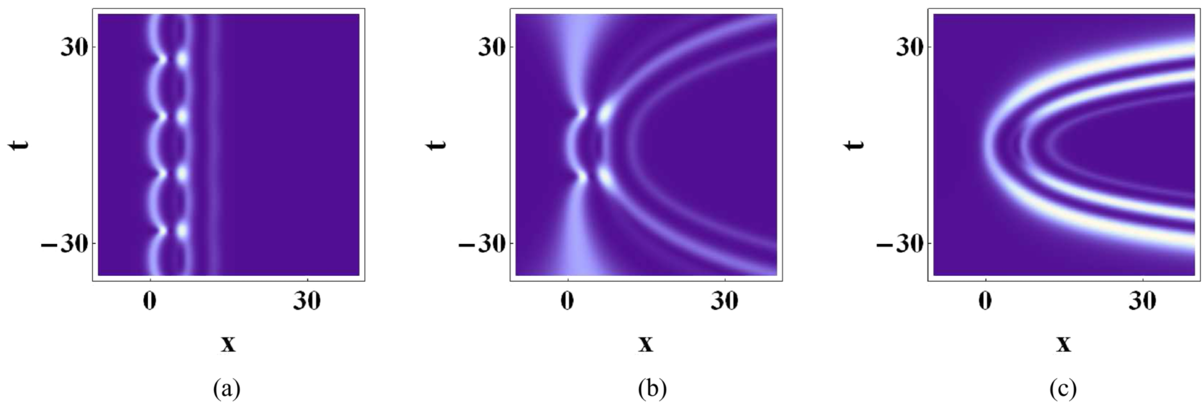

FIG. 3. (Color online) Density plots of the bound interaction between two solitons formed by $|\psi_1|^2$ via expressions (8) and (14) with the parameters $\Gamma(t) = \rho_1 \tanh(2\rho_1 t)$, $\tau_1 = 0.8$, $\tau_2 = 1$, $\beta_1^{(1)} = \beta_2^{(1)} = 0.5$, $\beta_1^{(0)} = \beta_2^{(0)} = 0.4$, $\beta_1^{(-1)} = \beta_2^{(-1)} = 0.3$, $\alpha_1 = \alpha_{-1} = -1$, and $w_1^{(0)} = w_2^{(0)} = 0$. (a) $\rho_1 = 0$; (b) $\rho_1 = 0.03$; (c) $\rho_1 = 0.06$.

ferromagnetic state ($\Omega_2 = 0$) [18,20] propagate under the control of the expulsive potential. In Fig. 1, the two solitons have a head-on interaction; the interaction between adjacent solitons is presented in Fig. 2. Furthermore, we find that the expulsive potential affects the interaction between adjacent solitons. By taking one component ψ_1 as an example, a detailed comparison is performed in Fig. 3 via different choices of parameter ρ_1. Thereinto, Fig. 3(a) shows the bound interaction between two polar solitons that propagate nearly parallel without an external trap potential. When ρ_1 increases in Figs. 3(b) and 3(c), the range of solitonic interaction becomes smaller, with the expulsive potential intensifying, and the solitons propagate, respectively, in the confinement of the trap potential.

B. Periodically modulated trap potential

When

$$U(t) = \frac{\rho_2 \widetilde{w} \cos(\widetilde{w} t + \theta_0) + \rho_2^2 [\cos(2\widetilde{w} t + 2\theta_0) - 1 + \widetilde{w}]}{2[1 + \rho_2 \cos(\widetilde{w} t + \theta_0)]^2},$$

$$\Gamma(t) = -\frac{\rho_2 \sin(\widetilde{w} t + \theta_0)}{1 + \rho_2 \cos(\widetilde{w} t + \theta_0)}, \tag{19}$$

we can perform propagation and interaction of the matter-wave solitons under a periodically modulated trap potential, where $|\rho_2| < 1$, $\widetilde{w}$, and θ_0 are, respectively, the amplitude, frequency, and starting phase of the modulation. To get explicit expressions for the characteristic lines, we take $\widetilde{w} = 2$ and $\theta_0 = 0$ for simplicity and derive

$$\begin{aligned} &\frac{x}{1 + \rho_2 \cos(2t)} \\ &\quad + (\tau_m - \tau_m^*) \left\{ \left(\rho_2^2 - 1\right)^{-\frac{3}{2}} \operatorname{arctanh}\left[\left(\frac{\rho_2 - 1}{\rho_2 + 1}\right)^{\frac{1}{2}} \tan(t)\right] \right. \\ &\quad \left. - \frac{\rho_2 \sin(2t)}{2\left(\rho_2^2 - 1\right)[1 + \rho_2 \cos(2t)]} \right\} + \frac{\widetilde{c}_m}{\tau_m + \tau_m^*} = 0, \\ &m = 1, 2. \end{aligned} \tag{20}$$

It is noted that the singular points exist in the characteristic lines if the imaginary parts of the τ_m ($m = 1, 2$) are nonzero. Thus, we illustrate the bound interaction between the polar and ferromagnetic solitons with real τ_m ($m = 1, 2$) in Fig. 4 and contrast the polar-polar solitonic interaction of one component ψ_1 via different ρ_2 values in Fig. 5. By comparison, we find that, besides the propagation path, the period of solitonic interaction can be modulated through the periodic trap potential.

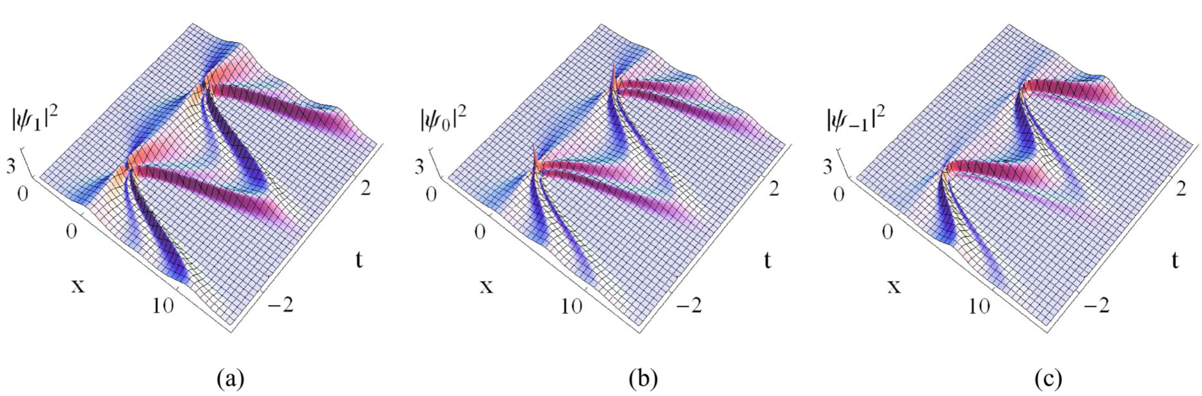

FIG. 4. (Color online) Bound interaction between the two solitons formed by $|\psi_j|^2$ ($j = 1, 0, -1$) via expressions (8) and (14) with the parameters $\Gamma(t) = -\rho_2 \sin(wt + \theta_0)/[1 + \rho_2 \cos(wt + \theta_0)]$, $\tau_1 = 1.2$, $\tau_2 = 1$, $\beta_1^{(1)} = 0.6$, $\beta_1^{(0)} = 0.5$, $\beta_1^{(-1)} = 0.3$, $\beta_2^{(1)} = 0.8$, $\beta_2^{(0)} = 0.5$, $\beta_2^{(-1)} = 0.3125$, $\alpha_1 = \alpha_{-1} = -1$, $w_1^{(0)} = w_2^{(0)} = 0$, $\widetilde{w} = 2$, $\theta_0 = 0$, and $\rho_2 = 0.8$.

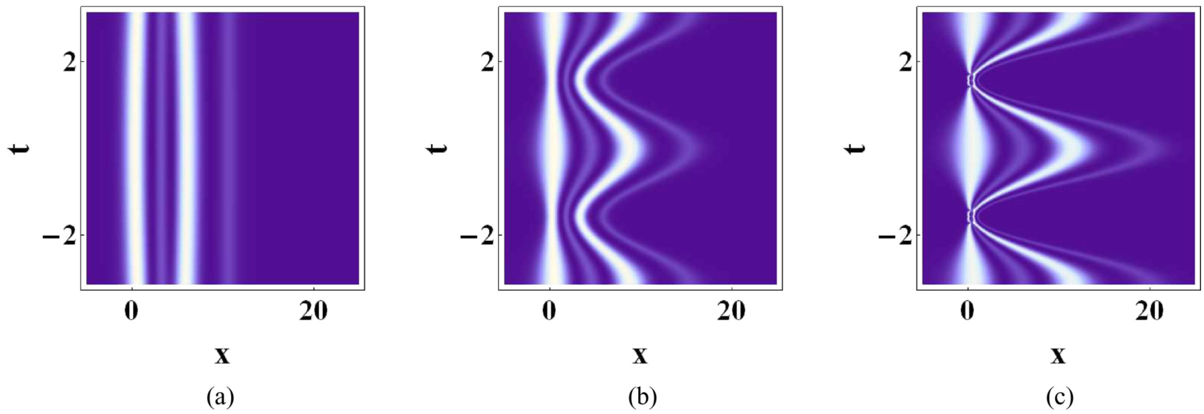

FIG. 5. (Color online) Density plots of the bound interaction between two solitons formed by $|\psi_1|^2$ via expressions (8) and (14) with the parameters $\Gamma(t) = -\rho_2 \sin(wt + \theta_0)/[1 + \rho_2 \cos(wt + \theta_0)]$, $\tau_1 = 1.2$, $\tau_2 = 1$, $\beta_1^{(1)} = 0.6$, $\beta_1^{(0)} = 0.5$, $\beta_1^{(-1)} = 0.3$, $\beta_2^{(1)} = 0.8$, $\beta_2^{(0)} = 0.5$, $\beta_2^{(-1)} = 0.3$, $\alpha_1 = \alpha_{-1} = -1$, $w_1^{(0)} = w_2^{(0)} = 0$, $\widetilde{w} = 2$, and $\theta_0 = 0$. (a) $\rho_2 = 0$; (b) $\rho_2 = 0.45$; (c) $\rho_2 = 0.9$.

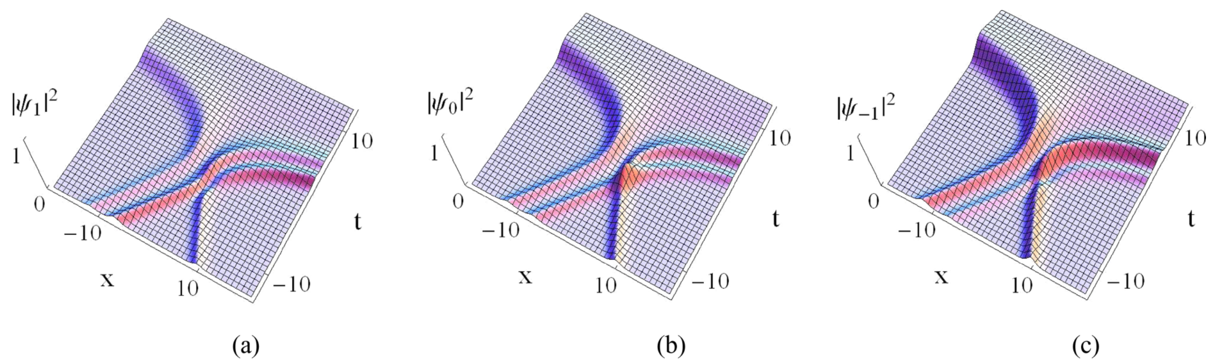

FIG. 6. (Color online) Head-on interaction between the two solitons formed by $|\psi_j|^2$ ($j = 1,0,-1$) via expressions (8) and (14) with the parameters $\Gamma(t) = \rho_3[1+\tanh(2\rho_3 t)]$, $\tau_1 = 0.4 + 0.3i$, $\tau_2 = 0.5-0.2i$, $\beta_1^{(1)} = 0.3$, $\beta_1^{(0)} = 0.4$, $\beta_1^{(-1)} = 0.5$, $\beta_2^{(1)} = 0.8$, $\beta_2^{(0)} = 1$, $\beta_2^{(-1)} = 1.25$, $\alpha_1 = \alpha_{-1} = -1$, $w_1^{(0)} = w_2^{(0)} = 0$, and $\rho_3 = 0.1$.

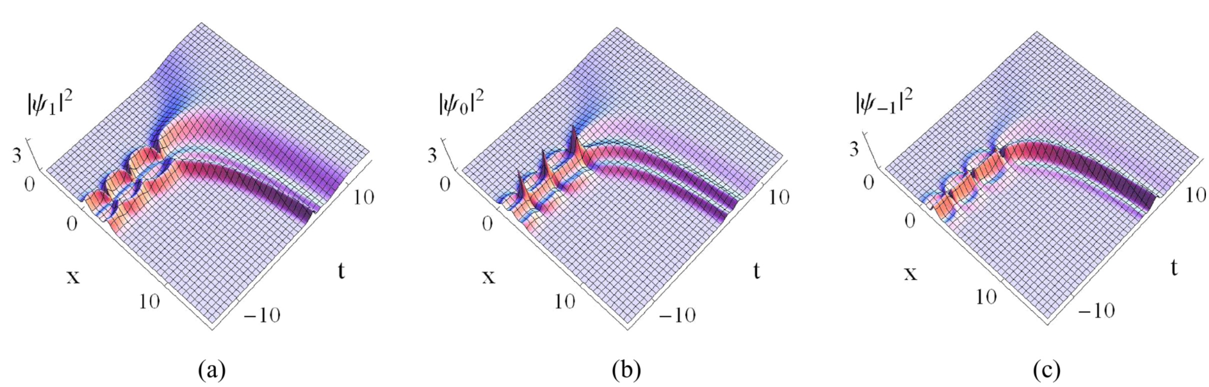

FIG. 7. (Color online) Bound interaction between the two solitons formed by $|\psi_j|^2$ (j=1,0,−1) via expressions (8) and (14) with the parameters $\Gamma(t) = \rho_3[1 + \tanh(2\rho_3 t)]$, $\tau_1 = 1.2$, $\tau_2 = 1$, $\beta_1^{(1)} = 0.6$, $\beta_1^{(0)} = 0.5$, $\beta_1^{(-1)} = 0.3$, $\beta_2^{(1)} = 0.8$, $\beta_2^{(0)} = 0.5$, $\beta_2^{(-1)} = 0.3125$, $\alpha_1 = \alpha_{-1} = -1, w_1^{(0)} = w_2^{(0)} = 0$, and $\rho_3 = 0.1$.

C. Kink-like-modulated trap potential

Next, we set $U(t) = -2\rho_3^2[1 + \tanh(2\rho_3 t)]$, which corresponds to a kink-like-modulated trap potential with a gain or loss term of $\Gamma(t) = \rho_3[1 + \tanh(2\rho_3 t)]$. Under that condition, the matter-wave solitons can keep their initial states until the external trap potential begins to take effect near $t = 0$, and the characteristic lines can be expressed as

$$\frac{2x}{1+e^{4\rho_3 t}} + (\tau_m - \tau_m^*) \times \left[\frac{1}{\rho_3}\ln(1+e^{4\rho_3 t}) - \frac{1}{\rho_3(1+e^{4\rho_3 t})} - 4t\right] + \frac{\widetilde{c}_m}{\tau_m + \tau_m^*} = 0, \quad m = 1, 2. \tag{21}$$

With the propagation path chosen via expression (21), the head-on interaction and bound interaction between a polar soliton and a ferromagnetic soliton are shown in Figs. 6 and 7, respectively. To get more details about the influence of the trap potential, we take the component ψ_1 and plot (in Fig. 8) the polar-polar solitonic interaction in three cases for $\rho_3 = 0$, $\rho_3 = 0.02$, and $\rho_3 = 0.04$. As ρ_3 increases, the period of solitonic interaction becomes short and the solitons separate from each other earlier. Under the constraint of an external trap potential, the solitons can propagate along their own paths and their interaction seems to be nearly eliminated after a period of time.

IV. NUMERICAL SIMULATION

By means of the time-splitting spectral method, which has been used to study coupled GP equations for spinor BECs [46–48], we numerically study the dynamic stability of the matter-wave solitons of Eqs. (5) under the condition of an expulsive potential and a constant gain or loss term. In the finite computational region $x \in [x_{\min}, x_{\max}]$ with periodic boundary condition $\psi_j(x_{\min},t) = \psi_j(x_{\max},t)$, we choose a spatial mesh size $\Delta x > 0$ and a temporal step size $\Delta t > 0$ for $\widetilde{N} = (x_{\max} - x_{\min})/\Delta x$ an even positive integer, and the grid points are given by $x_k = x_{\min} + k\Delta x$ $(k = 0, 1, 2, \ldots, \widetilde{N} - 1)$ and $t_n = n\Delta t$ $(n = 0, 1, 2, \ldots)$. In the simulation, with an initial random noise added to the initial data $\psi_j(x_k,0)$ $(j = -1, 0, 1, k = 1, 2, \ldots, \widetilde{N} - 1)$, the evolution of the densities $|\psi_j(x,t)|^2$, numbers of the three components, $N_j = \int_{-\infty}^{+\infty} |\psi_j(x,t)|^2 dx$ $(j = -1, 0, 1)$, total number $N_{\rm tot} = N_1 + N_0 + N_{-1}$, and magnetization $N_1 - N_{-1}$ in different cases will be illustrated. Because of the atom gain or loss, the atom numbers are no longer conserved, and we can derive

$$N_j(t) = N_j(t)|_{t=0}\, e^{2\int_0^t \Gamma(\gamma)d\gamma}, \quad j = -1, 0, 1. \tag{22}$$

From expressions (8) and (13), we first examine the stability of one-soliton solutions in the ferromagnetic state and polar state, respectively. For accuracy of computation, we set the positions of the solitons to minimize their amplitudes and phases on the boundary. It can be observed from Figs. 9 and 10 that the evolutions of both the ferromagnetic soliton and polar soliton can be dynamically stable under the effect of additional random noise, and atom numbers can be accurately predicted via expression (22).

To examine the robustness of solitonic interaction, we perform a head-on interaction and a bound interaction between a ferromagnetic soliton and a polar soliton under the same external trap potential as above. For the head-on interaction, the initial condition is given by $\psi_j^{\rm mix}(x_k,0) = \psi_j^{\rm ferro}(x_k,0) + \psi_j^{\rm polar}(x_k,0)$ $(j = -1, 0, 1, k = 1, 2, \ldots, \widetilde{N} - 1)$, where $\psi_j^{\rm ferro}(x_k,0)$ and $\psi_j^{\rm polar}(x_k,0)$ correspond to the initial data of the ferromagnetic soliton and the polar soliton, respectively, and the two solitons should be separated far from each other initially to ensure that there is hardly any interaction between them. For the bound interaction, we set the initial condition from expressions (8) and (14).

As shown in Figs. 11, 12, and 13, the evolutions of two solitons including two types of interaction (the head-on interaction and bound interaction) are stable with a perturbation of 5% random noise in the numerical simulation. From the evolution of N_1 (solid blue line) and N_0 (dotted red line), we can investigate the spin-exchange interaction during the two-soliton interaction.

In the case of the head-on interaction, we can hardly find evidence for spin-exchange interaction from Fig. 11 when the solitons propagate at a higher speed; on the other hand, the spin-exchange interaction occurs in Fig. 12 while two lower-speed solitons interact with each other, and the proportion of atom numbers of the three components is redistributed after the interaction.

When the bound interaction between two adjacent solitons arises, continual spin-exchange interaction can be observed (Fig. 13). Under the effect of relevant atom loss, expulsive potential, and nonlinearity, the period of the bound interaction is no longer a constant, as seen in Figs. 3(a) and 8(a), but turns to be a varied one in Fig. 13. Simultaneously, the frequency of the spin-exchange interaction increases and the atoms of the three components interchange more rapidly due to the time-dependent modulation in the nonautonomous BEC system. More on the solitonic interactions can be seen, e.g., in Refs. [49–54].

V. ROGUE-WAVE-LIKE SOLUTIONS OF EQS. (5)

Moreover, under constraints (7) and (11), we also derive rogue-wave-like solutions of Eqs. (5) in the following forms:

$$\psi_j = \mu_j \left\{1 + \frac{\delta_j\,[1 + L(t)\,i\,]}{P(t)\,x^2 + Q(t)\,x + R(t)}\right\} e^{[-\frac{1}{2}\Gamma(t)x^2 + W(t)]\,i}, \quad j = -1, 0, 1, \tag{23}$$

where μ_j and δ_j $(j = -1, 0, 1)$ are real parameters, and $L(t)$, $P(t)$, $Q(t)$, $R(t)$, and $W(t)$ are real functions with respect to t. There are two cases of undetermined quantities to be discussed.

(1) When $\mu_0^2 = \mu_1\,\mu_{-1}$,

$$\begin{aligned}
&\xi_1 = \alpha_{-1}\,\mu_{-1}^2 + \alpha_0\,\mu_0^2 + \alpha_1\,\mu_1^2, \quad \delta_1 = \delta_{-1} = \delta_0,\\
&P(t) = -\frac{1}{2}\,\delta_0\,\xi_1\,e^{-4\int\Gamma(t)dt}, \quad Q(t) = \sigma_1\,e^{-2\int\Gamma(t)dt},\\
&W(t) = -\int \frac{2\,P(t)}{\delta_0}dt, \quad L(t) = -\int \frac{4\,P(t)}{\delta_0}dt,\\
&R(t) = -\frac{1}{4}\,\delta_0\,[1 + L(t)^2] - \frac{\sigma_1^2}{2\,\delta_0\,\xi_1}.
\end{aligned} \tag{24}$$

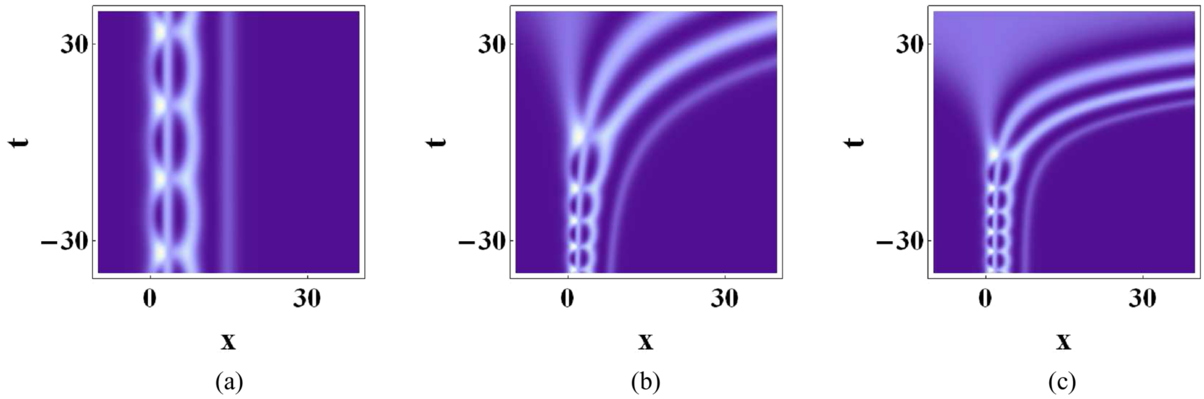

FIG. 8. (Color online) Density plots of the bound interaction between two solitons formed by $|\psi_1|^2$ via expressions (8) and (14) with the parameters $\Gamma(t) = \rho_3[1 + \tanh(2\rho_3 t)]$, $\tau_1 = 0.8$, $\tau_2 = 0.6$, $\beta_1^{(1)} = 0.1$, $\beta_1^{(0)} = 0.4$, $\beta_1^{(-1)} = 0.3$, $\beta_2^{(1)} = 0.5$, $\beta_2^{(0)} = 0.4$, $\beta_2^{(-1)} = 0.3$, $\alpha_1 = \alpha_{-1} = -1$,and $w_1^{(0)} = w_2^{(0)} = 0$. (a) $\rho_3 = 0$; (b) $\rho_3 = 0.015$; (c) $\rho_3 = 0.03$.

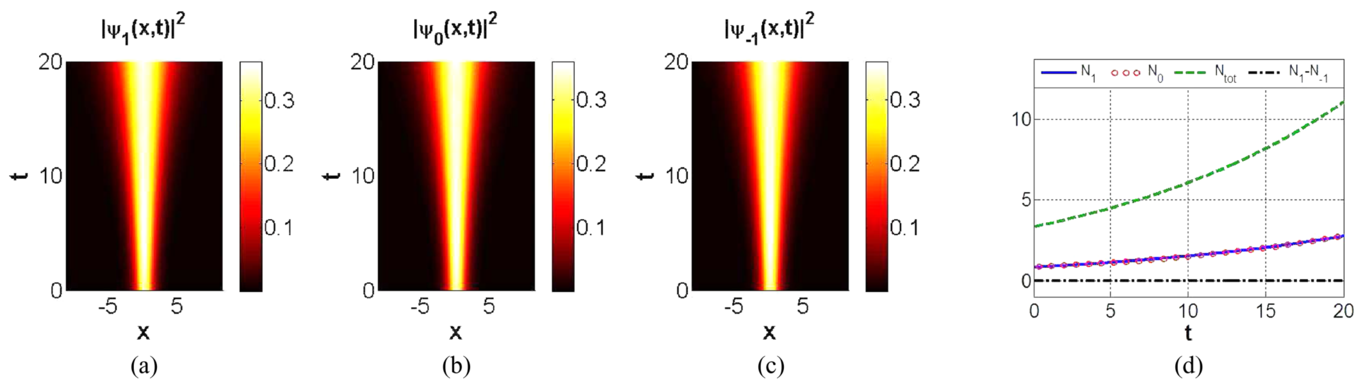

FIG. 9. (Color online) (a)–(c) Density evolution of the three components. (d) Evolution of the numbers of the three components, total number, and magnetization. Initial data in the numerical simulation are derived from expressions (8) and (13) with a random noise level of 5% added. Here we choose $x_{\min} = -24$, $x_{\max} = 24$, $\widetilde{N} = 2^{11}$, $\Delta t = 0.001$, and $T = 20$, and other parameters are given by $\Gamma(t) = 0.03$, $\alpha_1 = \alpha_{-1} = -1$, $\tau_1 = 0.8$, $w_1(t)|_{t=0} = -0.5i$, and $\beta_1^{(1)} = \beta_1^{(0)} = \beta_1^{(-1)} = 0.7$. The N_{tot} values are 3.35, 6.10, and 11.11 at $t = 0$, 10, and 20, respectively.

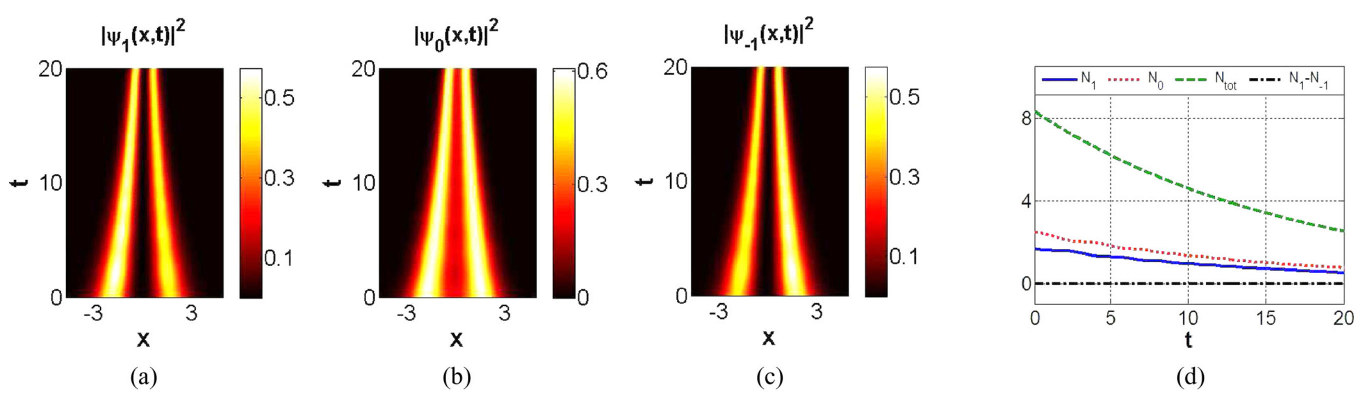

FIG. 10. (Color online) (a)–(c) Density evolution of the three components. (d) Evolution of the numbers of the three components, total number, and magnetization. Initial data in the numerical simulation are derived from expressions (8) and (13) with a random noise level of 5% added. Here we choose $x_{\min} = -24$, $x_{\max} = 24$, $\widetilde{N} = 2^{11}$, $\Delta t = 0.001$, and $T = 20$, and other parameters are given by $\Gamma(t) = -0.03$, $\alpha_1 = \alpha_{-1} = -1$, $\tau_1 = 1$, $w_1(t)|_{t=0} = -2.4i$, $\beta_1^{(1)} = \beta_1^{(0)} = 1$, and $\beta_1^{(-1)} = 0.9$. The N_{tot} values are 8.36, 4.58, and 2.52 at $t = 0$, 10, and 20, respectively.

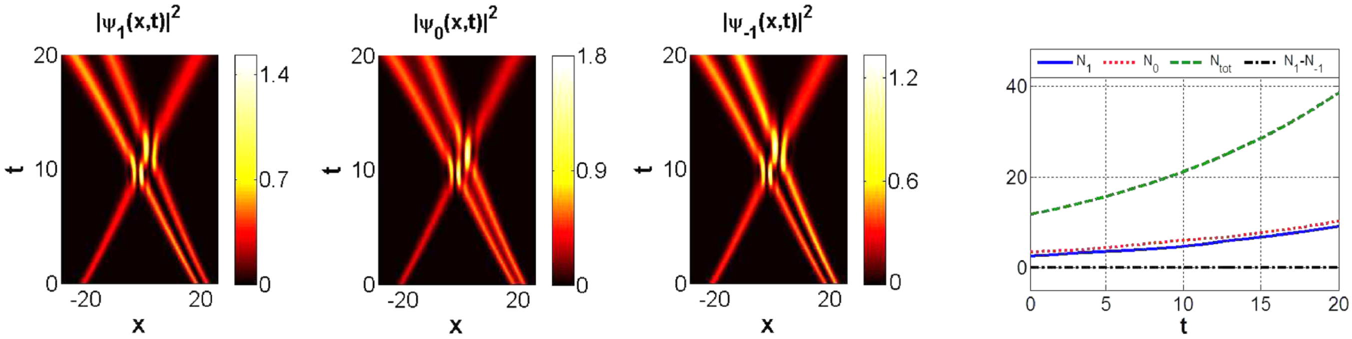

(a) (b) (c) (d)

FIG. 11. (Color online) (a)–(c) Density evolution of the three components. (d) Evolution of the numbers of the three components, total number, and magnetization. Initial data in the numerical simulation are given by $\psi_j^{\mathrm{mix}}(x_k,0)$'s ($j=-1,0,1$, $k=1,2,\ldots,\widetilde{N}-1$) with a random noise level of 5% added. Here we choose $x_{\min}=-48$, $x_{\max}=48$, $\widetilde{N}=2^{12}$, $\Delta t=0.001$, and $T=20$, and other parameters are given by $\Gamma(t)=0.03$, $\alpha_1=\alpha_{-1}=-1$, $\tau_1=0.8+1.8i$, $w_1(t)|_{t=0}=-18i$, $\beta_1^{(1)}=\beta_1^{(0)}=\beta_1^{(-1)}=0.7$, $\tau_2=1-1.7i$, $w_2(t)|_{t=0}=18i$, and $\beta_2^{(1)}=\beta_2^{(0)}=1,\beta_2^{(-1)}=0.9$. The N_{tot} values are 11.70, 21.32, and 38.85 at $t=0$, 10, and 20, respectively.

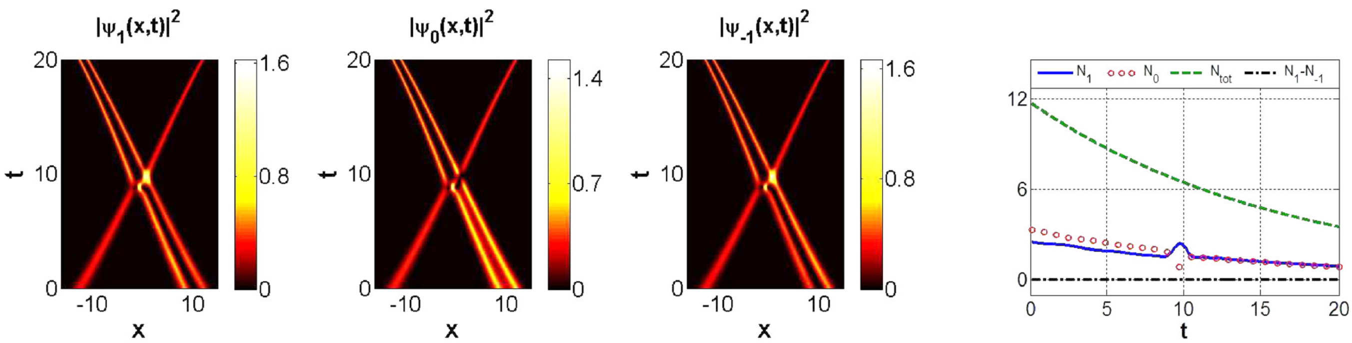

(a) (b) (c) (d)

FIG. 12. (Color online) (a)–(c) Density evolution of the three components. (d) Evolution of the numbers of the three components, total number, and magnetization. Initial data in the numerical simulation are given by $\psi_j^{\mathrm{mix}}(x_k,0)$'s ($j=-1,0,1$, $k=1,2,\ldots,\widetilde{N}-1$) with a random noise level of 5% added. Here we choose $x_{\min}=-28$, $x_{\max}=28$, $\widetilde{N}=2^{12}$, $\Delta t=0.001$, and $T=20$, and other parameters are given by $\Gamma(t)=-0.03$, $\alpha_1=\alpha_{-1}=-1$, $\tau_1=0.8+0.3i$, $w_1(t)|_{t=0}=-11i$, $\beta_1^{(1)}=\beta_1^{(0)}=\beta_1^{(-1)}=0.7$, $\tau_2=1-0.3i, w_2(t)|_{t=0}=8i$, and $\beta_2^{(1)}=\beta_2^{(0)}=1,\beta_2^{(-1)}=0.9$. The N_{tot} values are 11.70, 6.42, and 3.52 at $t=0$, 10, and 20, respectively.

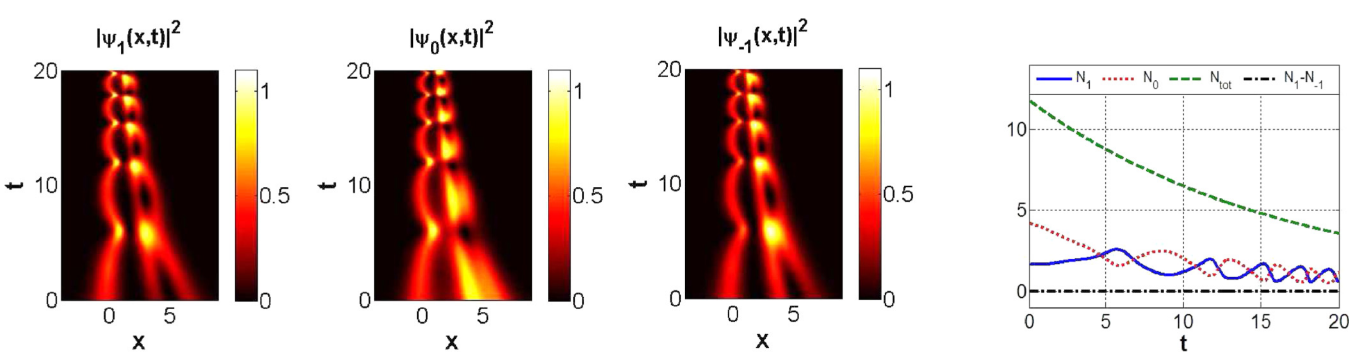

(a) (b) (c) (d)

FIG. 13. (Color online) (a)–(c) Density evolution of the three components. (d) Evolution of the numbers of the three components, total number, and magnetization. Initial data in the numerical simulation are derived from expressions (8) and (14) with a random noise level of 5% added. Here we choose $x_{\min}=-28$, $x_{\max}=28$, $\widetilde{N}=2^{12}$, $\Delta t=0.001$, and $T=20$, and other parameters are given by $\Gamma(t)=-0.03$, $\alpha_1=\alpha_{-1}=-1$, $\tau_1=0.8$, $w_1(t)|_{t=0}=0$, $\beta_1^{(1)}=\beta_1^{(0)}=\beta_1^{(-1)}=0.7$, $\tau_2=1$, $w_2(t)|_{t=0}=0$, $\beta_2^{(1)}=\beta_2^{(0)}=1$, and $\beta_2^{(-1)}=0.9$. The N_{tot} values are 11.76, 6.46, and 3.54 at $t=0$, 10, and 20, respectively.

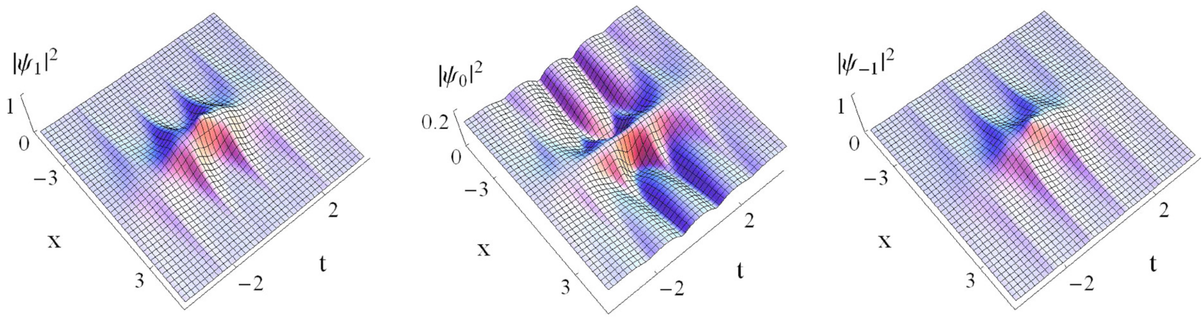

(a) (b) (c)

FIG. 14. (Color online) Rogue waves in the periodic oscillation formed by $|\psi_j|^2$ ($j = 1,0,-1$) via expressions (23) and (25) with the parameters $\Gamma(t) = 0.7\sin(4t)/[1 + 0.7\cos(4t)]$, $\delta_0 = 1$, $\mu_1 = 0.15$, $\mu_0 = 0.4$, $\mu_{-1} = -0.25$, $\sigma_2 = 0$, and $\alpha_0 = -4$.

(2) When $\mu_0^2 \neq \mu_1\,\mu_{-1}$,

$$\frac{\mu_1}{\mu_{-1}} = -\frac{\alpha_0}{2\alpha_1} = -\frac{2\alpha_{-1}}{\alpha_0}, \quad \xi_2 = \alpha_{-1}\,\mu_{-1}^2 + \alpha_0\,\mu_0^2 + \alpha_1\,\mu_1^2,$$

$$\delta_1 = \delta_0\left[1 \mp \frac{\sqrt{-\mu_1\,\mu_{-1}\left(\mu_0^2 - \mu_1\,\mu_{-1}\right)}}{\mu_1\,\mu_{-1}}\right],$$

$$\delta_{-1} = \delta_0\left[1 \pm \frac{\sqrt{-\mu_1\,\mu_{-1}\left(\mu_0^2 - \mu_1\,\mu_{-1}\right)}}{\mu_1\,\mu_{-1}}\right],$$

$$P(t) = -\frac{1}{2}\,\delta_0\,\xi_2\,e^{-4\int\Gamma(t)dt}, \quad Q(t) = \sigma_2\,e^{-2\int\Gamma(t)dt},$$

$$W(t) = -\int\frac{P(t)}{\delta_0}dt, \quad L(t) = -\int\frac{2\,P(t)}{\delta_0}dt,$$

$$R(t) = -\frac{1}{2}\,\delta_0\,[1 + L(t)^2] - \frac{\sigma_2^2}{2\,\delta_0\,\xi_2}. \tag{25}$$

It is noted that expressions (24) correspond to the rogue-wave-like solutions with the three components ψ_j ($j = -1, 0, 1$) evolving in the same shape, so we pay attention to solutions (23) with the quantities satisfying expressions (25) only when $\mu_0^2 \neq \mu_1\,\mu_{-1}$. Under the influence of a periodically modulated trap potential and a periodic atom gain or loss, the rogue waves can emerge in the superposition of localized character and periodic oscillating properties as shown in Fig. 14. Different from the other two "bright" components ψ_1 and ψ_{-1}, the middle component ψ_0 can evolve like a nonautonomous rogue wave in the "dark" shape.

VI. CONCLUSIONS

As the mean-field approximation for the dynamics of the one-dimensional trapped spin-1 BEC with a time-dependent external trap potential and atom gain or loss, Eqs. (5) have been investigated in this paper. Under constraints (7) and (11), soliton solutions (13) and (14) through transformations (8) have been derived by means of bilinear forms (9), and rogue-wave-like solutions (23) of Eqs. (5) have also been obtained. Via different choices of parameters, we have calculated the propagation and interaction of nonautonomous matter-wave solitons and determined the evolution of nonautonomous rogue waves in Figs. 1–14 under the respective effects of a expulsive potential, a periodically modulated trap potential, and a kink-like-modulated trap potential. From the illustrations, we have the following conclusions for Eqs. (5):

(i) Through the derivation of expressions (18), (20), and (21) for the characteristic lines, we have found that the external trap potential and atom gain or loss can influence the propagation of matter-wave solitons, but they have little effect on the head-on solitonic interaction, as shown in Figs. 1 and 6.

(ii) From Figs. 2, 4, and 7, we have observed that the duration and frequency of the bound solitonic interaction can be influenced by the external trap potential and atom gain or loss. Investigating Figs. 3, 5, and 8, we have found that the stronger the expulsive potential is, the shorter the duration of bound interaction that can be observed (as seen in Fig. 3); in the case of the periodically modulated trap potential, the frequency of the bound interaction will approach that of the external trap potential (as seen in Fig. 5); for the kink-like-modulated trap potential, the bound interaction will experience a higher frequency and vanish earlier when the external trap potential becomes stronger (as seen in Fig. 8).

(iii) By means of numerical simulation, it can be seen that taking the expulsive potential and constant gain or loss term as an example, we have realized the stable evolution of a ferromagnetic soliton and a polar soliton, including their propagation (as seen in Figs. 9 and 10), head-on interaction (as seen in Figs. 11 and 12), and bound interaction (as seen in Fig. 13) with a perturbation of 5% initial random noise. The spin-exchange interaction of atoms, which is related to the interaction of matter-wave solitons, can be affected by the time-dependent modulation in the nonautonomous BEC system.

(iv) Under the influence of a periodically modulated trap potential and periodic atom gain or loss, rogue waves, including "bright" and "dark" shapes, can emerge in the superposition of localized character and periodic oscillating properties, as shown in Fig. 14.

ACKNOWLEDGMENTS

We express our sincere thanks to the referees and all the members of our discussion group for their valuable comments. This work has been supported by the National Natural Science Foundation of China under Grant No. 11272023 and by the Open Fund of State Key Laboratory of Information Photonics and Optical Communications (Beijing University of Posts and Telecommunications) under Grant No. IPOC2013B008.

APPENDIX

With the subscripts $m, n = 1, 2$, the quantities in expressions (13) and (14) are presented as follows:

$$\Lambda^{(j_1,\, j_2)} = \beta_1^{(j_1)}\beta_2^{(j_2)} + \beta_1^{(j_2)}\beta_2^{(j_1)}, \quad j_1, j_2 = -1, 0, 1, \tag{A1}$$

$$\Theta_{m,\,n} = \alpha_1\beta_m^{(1)}\beta_n^{(1)*} + \alpha_0\beta_m^{(0)}\beta_n^{(0)*} + \alpha_{-1}\beta_m^{(-1)}\beta_n^{(-1)*}, \tag{A2}$$

$$b_{mn} = -\frac{\Theta_{m,\,n}}{2\,(\tau_m + \tau_n^*)^2}, \tag{A3}$$

$$c_{mn}^{(j)} = -\frac{(-2)^{|j|}\,\alpha_{-j}\,\Omega_m\,\beta_n^{(-j)*}}{4\,(\tau_m + \tau_n^*)^2}, \quad j = -1, 0, 1, \tag{A4}$$

$$c_m^{(j)} = \frac{1}{2\,(\tau_1 + \tau_m^*)\,(\tau_2 + \tau_m^*)}\left[\alpha_{-j}\,\Lambda^{(0,\,0)}\beta_m^{(-j)*} + \alpha_0\,\Lambda^{(j,\,0)}\beta_m^{(0)*} + \alpha_j\,\Lambda^{(j,\,j)}\beta_m^{(j)*}\right], \quad j = \pm 1, \tag{A5}$$

$$c_m^{(0)} = \frac{1}{4\,(\tau_1 + \tau_m^*)\,(\tau_2 + \tau_m^*)}\left\{2\,\alpha_{-1}\,\Lambda^{(0,\,-1)}\beta_m^{(-1)*} + \alpha_0\beta_m^{(0)*}[\Lambda^{(0,\,0)} + \Lambda^{(1,\,-1)}] + 2\,\alpha_1\,\Lambda^{(1,\,0)}\beta_m^{(1)*}\right\}, \tag{A6}$$

$$d_{mn} = \frac{\alpha_0^2\,\Omega_m\,\Omega_n^*}{16\,(\tau_m + \tau_n^*)^4}, \tag{A7}$$

$$d_m = \frac{\alpha_0^2\,\Omega_m\,[\Lambda^{(0,\,0)*} - \Lambda^{(1,\,-1)*}]}{16\,(\tau_m + \tau_1^*)^2\,(\tau_m + \tau_2^*)^2}, \tag{A8}$$

$$d_0 = \frac{\alpha_0^2\,|\Lambda^{(0,\,0)} - \Lambda^{(1,\,-1)}|^2 - 4\,(\Theta_{1,\,1}\,\Theta_{2,\,2} + \Theta_{1,\,2}\,\Theta_{2,\,1})}{16\,(\tau_1 + \tau_1^*)\,(\tau_1 + \tau_2^*)\,(\tau_2 + \tau_1^*)\,(\tau_2 + \tau_2^*)}, \tag{A9}$$

$$l_{mn}^{(j)} = \frac{\alpha_0^2\,\beta_{3-m}^{(j)}\,\Omega_m\,\Omega_n^*\,(\tau_1 - \tau_2)^2}{16\,(\tau_1 + \tau_n^*)^2\,(\tau_2 + \tau_n^*)^2\,(\tau_m + \tau_n^*)^2}, \quad j = -1, 0, 1, \tag{A10}$$

$$l_m^{(j)} = -\frac{(-2)^{|j|}\,\alpha_{-j}\,\Omega_{3-m}\,(\tau_1 - \tau_2)^2}{4\,(\tau_{3-m} + \tau_1^*)^2\,(\tau_{3-m} + \tau_2^*)^2}\left[c_m^{(-j)*} + \sum_{n=1}^{2} b_{mn}\,\beta_{3-n}^{(-j)*}\right], \quad j = -1, 0, 1, \tag{A11}$$

$$q_{mn} = -\frac{\alpha_0^2\,\Omega_m\,\Omega_n^*\,|\tau_1 - \tau_2|^4\,\Theta_{3-m,\,3-n}}{32\,(\tau_1 + \tau_1^*)^2\,(\tau_1 + \tau_2^*)^2\,(\tau_2 + \tau_1^*)^2\,(\tau_2 + \tau_2^*)^2\,(\tau_m + \tau_n^*)^2}, \tag{A12}$$

$$p_m^{(j)} = -\frac{(-2)^{|j|}\,\alpha_{-j}\,\beta_{3-m}^{(-j)*}\,\alpha_0^2\,\Omega_{3-m}\,|\Omega_m|^2\,(\tau_1 - \tau_2)^2\,|\tau_1 - \tau_2|^4}{64\,(\tau_1 + \tau_m^*)^4\,(\tau_2 + \tau_m^*)^4\,(\tau_1 + \tau_{3-m}^*)^2\,(\tau_2 + \tau_{3-m}^*)^2}, \quad j = -1, 0, 1, \tag{A13}$$

$$q_0 = \frac{\alpha_0^4\,|\Omega_1|^2\,|\Omega_2|^2\,|\tau_1 - \tau_2|^8}{256\,(\tau_1 + \tau_1^*)^4\,(\tau_1 + \tau_2^*)^4\,(\tau_2 + \tau_1^*)^4\,(\tau_2 + \tau_2^*)^4}, \tag{A14}$$

$$h_{mn} = -\frac{(\tau_1 - \tau_2)^2\,\Omega_{3-m}\,\Theta_{m,\,n}}{2\,(\tau_1 + \tau_n^*)^2\,(\tau_2 + \tau_n^*)^2}, \tag{A15}$$

$$h_m = \frac{\alpha_0^2\,(\tau_1 - \tau_2)^4\,\Omega_{3-m}\,|\Omega_m|^2}{16\,(\tau_1 + \tau_m^*)^4\,(\tau_2 + \tau_m^*)^4}, \tag{A16}$$

$$h_0 = \frac{\alpha_0^2\,(\tau_1 - \tau_2)^4\,\Omega_1\,\Omega_2\,[\Lambda^{(0,\,0)*} - \Lambda^{(1,\,-1)*}]}{16\,(\tau_1 + \tau_1^*)^2\,(\tau_1 + \tau_2^*)^2\,(\tau_2 + \tau_1^*)^2\,(\tau_2 + \tau_2^*)^2}. \tag{A17}$$

[1] A. Griffin, D. W. Snoke, and S. Stringari, *Bose-Einstein Condensation* (Cambridge University Press, Cambridge, England, 1995).

[2] M. H. Anderson, J. R. Ensher, M. R. Matthews, C. E. Wieman, and E. A. Cornell, Science **269**, 198 (1995).

[3] K. B. Davis, M. O. Mewes, M. R. Andrews, N. J. van Druten, D. S. Durfee, D. M. Kurn, and W. Ketterle, Phys. Rev. Lett. **75**, 3969 (1995).

[4] C. C. Bradley, C. A. Sackett, J. J. Tollett, and R. G. Hulet, Phys. Rev. Lett. **75**, 1687 (1995).

[5] D. G. Fried, T. C. Killian, L. Willmann, D. Landhuis, S. C. Moss, D. Kleppner, and T. J. Greytak, Phys. Rev. Lett. **81**, 3811 (1998).

[6] A. Robert, O. Sirjean, A. Browaeys, J. Poupard, S. Nowak, D. Boiron, C. I. Westbrook, and A. Aspect, Science **292**, 461 (2001).

[7] G. Modugno, G. Ferrari, G. Roati, R. J. Brecha, A. Simoni, and M. Inguscio, Science **294**, 1320 (2001).
[8] D. M. Stamper-Kurn, M. R. Andrews, A. P. Chikkatur, S. Inouye, H. J. Miesner, J. Stenger, and W. Ketterle, Phys. Rev. Lett. **80**, 2027 (1998).
[9] T. L. Ho, Phys. Rev. Lett. **81**, 742 (1998).
[10] T. Ohmi and K. Machida, J. Phys. Soc. Jpn. **67**, 1822 (1998).
[11] Y. Kawaguchi and M. Ueda, Phys. Rep. **520**, 253 (2012).
[12] V. Pietilä, M. Möttönen, and S. M. M. Virtanen, Phys. Rev. A **76**, 023610 (2007).
[13] M. Matuszewski, T. J. Alexander, and Y. S. Kivshar, Phys. Rev. A **80**, 023602 (2009).
[14] K. E. Strecker, G. B. Partridge, A. G. Truscott, and R. G. Hulet, Nature (London) **417**, 150 (2002).
[15] L. Khaykovich, F. Schreck, G. Ferrari, T. Bourdel, J. Cubizolles, L. D. Carr, Y. Castin, and C. Salomon, Science **296**, 1290 (2002).
[16] C. J. Pethick and H. Smith, *Bose-Einstein Condensation in Dilute Gases* (Cambridge University Press, Cambridge, England, 2002).
[17] Z. H. Zhang, C. Zhang, S. J. Yang, and S. Feng, J. Phys. B **45**, 215302 (2012).
[18] J. Ieda, T. Miyakawa, and M. Wadati, Phys. Rev. Lett. **93**, 194102 (2004).
[19] T. Kanna, K. Sakkaravarthi, C. S. Kumar, M. Lakshmanan, and M. Wadati, J. Math. Phys. **50**, 113520 (2009).
[20] M. Wang, B. Tian, W. R. Shan, X. Lü, and Y. S. Xue, Nonlinear Dyn. **69**, 1137 (2012).
[21] Z. Qin and G. Mu, Phys. Rev. E **86**, 036601 (2012).
[22] E. Tiesinga, B. J. Verhaar, and H. T. C. Stoof, Phys. Rev. A **47**, 4114 (1993).
[23] A. J. Moerdijk, B. J. Verhaar, and A. Axelsson, Phys. Rev. A **51**, 4852 (1995).
[24] P. O. Fedichev, Yu. Kagan, G. V. Shlyapnikov, and J. T. M. Walraven, Phys. Rev. Lett. **77**, 2913 (1996).
[25] J. L. Bohn and P. S. Julienne, Phys. Rev. A **56**, 1486 (1997).
[26] Ph. Courteille, R. S. Freeland, D. J. Heinzen, F. A. van Abeelen, and B. J. Verhaar, Phys. Rev. Lett. **81**, 69 (1998).
[27] J. L. Roberts, N. R. Claussen, J. P. Burke, C. H. Greene, E. A. Cornell, and C. E. Wieman, Phys. Rev. Lett. **81**, 5109 (1998).
[28] M. Olshanii, Phys. Rev. Lett. **81**, 938 (1998).
[29] J. Stenger, S. Inouye, M. R. Andrews, H.-J. Miesner, D. M. Stamper-Kurn, and W. Ketterle, Phys. Rev. Lett. **82**, 2422 (1999).
[30] S. L. Cornish, N. R. Claussen, J. L. Roberts, E. A. Cornell, and C. E. Wieman, Phys. Rev. Lett. **85**, 1795 (2000).
[31] S. Rajendran, P. Muruganandam, and M. Lakshmanan, J. Phys. B **42**, 145307 (2009).
[32] S. Rajendran, M. Lakshmanan, and P. Muruganandam, J. Math. Phys. **52**, 023515 (2011).
[33] V. R. Kumar, R. Radha, and M. Wadati, Phys. Lett. A **374**, 3685 (2010).
[34] S. Rajendran, P. Muruganandam, and M. Lakshmanan, Physica D **239**, 366 (2010).
[35] V. N. Serkin, A. Hasegawa, and T. L. Belyaeva, Phys. Rev. Lett. **98**, 074102 (2007).
[36] C. Hernandez-Tenorio, T. L. Belyaeva, and V. N. Serkin, Physica B **398**, 460 (2007).
[37] V. N. Serkin, A. Hasegawa, and T. L. Belyaeva, Phys. Rev. A **81**, 023610 (2010).
[38] L. C. Zhao, Z. Y. Yang, L. M. Ling, and J. Liu, Phys. Lett. A **375**, 1839 (2011).
[39] Z. Y. Yang, L. C. Zhao, T. Zhang, X. Q. Feng, and R. H. Yue, Phys. Rev. E **83**, 066602 (2011).
[40] L. C. Zhao, Ann. Phys. (NY) **329**, 73 (2013).
[41] L. Wen, L. Li, Z. D. Li, S. W. Song, X. F. Zhang, and W. M. Liu, Eur. Phys. J. D **64**, 473 (2011).
[42] J. Janis, M. Banks, and N. P. Bigelow, Phys. Rev. A **71**, 013422 (2005).
[43] R. Hirota, *The Direct Method in Soliton Theory* (Springer, Berlin, 1980).
[44] A. Veksler and Y. Zarmi, Physica D **211**, 57 (2005).
[45] Z. Y. Sun, Y. T. Gao, X. Yu, X. H. Meng, and Y. Liu, Wave Motion **46**, 511 (2009).
[46] W. Bao, S. Jin, and P. A. Markowich, J. Comput. Phys. **175**, 487 (2002).
[47] W. Bao, D. Jaksch, and P. A. Markowich, J. Comput. Phys. **187**, 318 (2003).
[48] H. Wang, Int. J. Comput. Math. **84**, 925 (2007).
[49] Y. Jiang, B. Tian, M. Li, and P. Wang, Nonlinear Dyn. **74**, 1053 (2013).
[50] H. L. Zhen, B. Tian, and W. R. Sun, Appl. Math. Lett. **27**, 90 (2014).
[51] H. L. Zhen, B. Tian, Y. F. Wang, H. Zhong, and W. R. Sun, Phys. Plasmas **21**, 012304 (2014).
[52] W. R. Sun, B. Tian, Y. Jiang, and H. L. Zhen, Ann. Phys. **343**, 215 (2014).
[53] W. R. Sun, B. Tian, H. Zhong, and H. L. Zhen, Stud. Appl. Math. **132**, 65 (2014).
[54] Y. Jiang and B. Tian, Europhys. Lett. **102**, 10010 (2013).